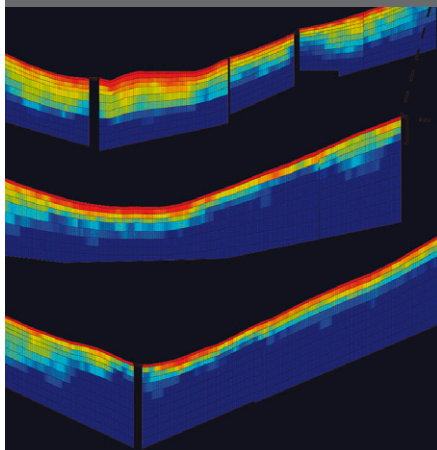


K.M. Befus*
A.F. Sheehan
M. Leopold
S.P. Anderson
R.S. Anderson



Seismic refraction surveys were used to characterize subsurface (0–20 m) critical zone structure in two variably eroded catchments. These geophysical snapshots show greater depth to fresh rock both on north-facing slopes in a steadily eroding catchment and in the headwaters of a catchment that has undergone recent fluvial incision at its base.

K.M. Befus, Campus Box 339, Dep. of Geological Sci., Univ. of Colorado, Boulder, CO 80309; A.F. Sheehan, M. Leopold, S.P. Anderson, and R.S. Anderson, Dep. of Geology, Univ. of Texas at Austin, 1 University Station C9000, Austin, TX 78712. *Corresponding author (Kevin. Befus@Colorado.edu).

Vadose Zone J. 10:915–927
doi:10.2136/vzj2010.0108
Received 27 Aug. 2010.
Posted online 29 July 2011.

© Soil Science Society of America
5585 Guilford Rd., Madison, WI 53711 USA.
All rights reserved. No part of this periodical may be reproduced or transmitted in any form or by any means, electronic or mechanical, including photocopying, recording, or any information storage and retrieval system, without permission in writing from the publisher.

Seismic Constraints on Critical Zone Architecture, Boulder Creek Watershed, Front Range, Colorado

We use a minimally invasive, shallow geophysical technique to image the structure of the critical zone from surface to bedrock (0–20 m) in two small drainages within the Boulder Creek Critical Zone Observatory (BcCZO). Shallow seismic refraction (SSR) surveys provide a three-dimensional network of two-dimensional cross-sections (termed *quasi-3D*) of critical zone compressional wave velocity (V_p) structure within each catchment, yielding a spatial description of the current critical zone structure. The two catchments, Betasso and Gordon Gulch, represent contrasting geomorphic histories within the Front Range: Betasso shows hillslope response to a late Cenozoic increase in fluvial incision of Boulder Creek, while Gordon Gulch represents more steady erosion. The mean depth to fresh bedrock in both catchments is roughly 15 m. Unique subsurface features in each catchment reflect active geomorphic processes not suggested by similarities in mean interface depths. Betasso contains thick disaggregated materials high in the drainage that are nearly absent near the outlet. This presumably reflects the impact of base-level lowering, which we suggest has progressed roughly 500 to 1000 m up into the catchment. Aspect-driven differences in the subsurface within each catchment add complexity and overprint the broader geomorphic signals. Shallow seismic refraction subsurface structure models will guide future investigations of critical zone processes from landscape to hydrologic modeling and are invaluable as connections between time-consuming point measurements of physical, chemical, and biological processes.

Abbreviations: BcCZO, Boulder Creek Critical Zone Observatory; ERT, electrical resistivity tomography; GPR, ground-penetrating radar; Ma, megaannum; quasi-3D, a three-dimensional grouping of two-dimensional surveys; SSR, shallow seismic refraction.

Shallow seismic refraction allows minimally invasive, broad spatial investigations of the subsurface (Leopold et al., 2008b). We use this geophysical technique to pair surficial evidence of geomorphic processes with physical and chemical weathering signatures interpreted from SSR surveys.

The interactions between weathering and transport processes sculpt terrestrial landscapes. Hillslope processes that include downslope movement of material by rain splash, frost creep, biological activity, and other gravity-driven mechanisms serve to redistribute material that is freed from the underlying bedrock by weathering processes. The hillslopes are in turn coupled to adjacent streams, which serve as their boundary conditions. This highly coupled geomorphic system therefore encompasses the majority of hydrological, geochemical, and biological activities that can all change in efficiency and in dominance through time.

Recently, the term *critical zone* (CZ) has been applied to the shallow terrestrial environment spanning from the lowest extent of groundwater to the top of the vegetation canopy (Brantley et al., 2007; Anderson et al., 2007) (Fig. 1). The definition of the CZ is inherently scale-dependent both spatially and in time. Within the CZ, rock evolves through various stages of decay and is overlain by soil and sediment. Together they support the local ecosystem. The properties of the weathered rock, sediment layers, and soil horizons, including biological activity, control water flow character, slope stability, active chemical reactions, and how the subterranean ecosystems interact with the local materials. Therefore, CZ structure exerts a first-order control on both subsurface and surface processes. Road and riverbank cuts, as well as cliff edges, allow partial insight into subsurface structure, but as these are unique hillslope boundary conditions they may not be representative of the broader hillslope. Quantitative descriptions of the three-dimensional CZ architecture can constrain both the potential volume and spatial distribution over which specific physical and chemical processes are either active or probable in the subsurface.

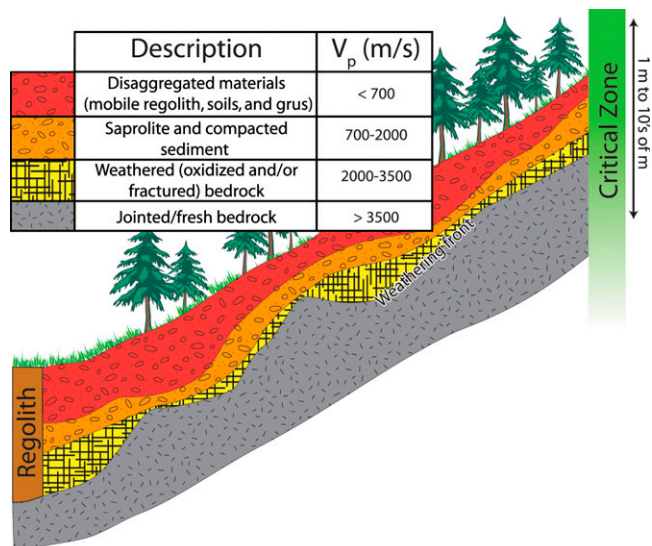


Fig. 1. The critical zone (CZ) spans from the lowest extent of groundwater flow to the top of the local vegetation canopy, requiring site-specific definition. We consider the CZ to extend through regolith and partially into fresh bedrock, where the transition from regolith to unweathered bedrock is defined as the bedrock weathering front. Estimates of V_p for each material composing the local CZ's geologic framework allow interpretation of shallow seismic refraction results.

In general we wish to avoid significantly altering the active processes in the attempt to quantify or understand them. Capturing the present architecture of the CZ without upsetting the system therefore becomes a challenge even where riverbanks, road cuts, and cliffs provide good insight into pieces of the geologic framework. Pits and trenches allow restricted insight into the structure and processes at depth, but once the material is replaced, the immediately adjacent system is likely to have been affected. Core collection results in a disturbed system with altered or enhanced water flow paths. Despite the potential disruption of the subsurface, boreholes, pits, and trenches are crucial for interpreting the results of shallow geophysical methods, where the geophysical signal of the subsurface can be matched with the physical properties and stratigraphy of the excavated materials. Geophysical surveys can guide such excavations to the most useful locations, potentially minimizing the number of disturbances. Geophysical surveys, anchored to physical measurements from limited excavations, can be applied over large areas to produce broad spatial coverage of the geologic framework to depths of tens of meters, quickly and cheaply.

Rock decays through a combination of physical, chemical, and biological processes, collectively termed *weathering*, that govern the evolution of the CZ. This disintegration and decomposition of rock supplies inorganic materials to the mobile layer that are then transported downslope. Previous studies of weathering either employ physical and/or chemical datasets from bedrock exposures, surface deposits, and boreholes or focus on the weathered character of soils (e.g., Birkeland et al., 2003; Dethier and Lazarus, 2006;

Egli et al., 2006; Rossi and Graham, 2010; Jin et al., 2010). These methods may fail to sample properly a target landscape and pair the results with either regional geomorphic processes or the character of bedrock weathering at depth. Jin et al. (2010) linked weathering and hillslope evolution at ridgetop locations with a single slope transect of soil cores. While geophysical surveys also allow us to explore finite volumes of the subsurface dependent on the survey setup, they can be applied across large, continuous profiles or three-dimensional volumes with minimal disturbance of the CZ.

Geophysical techniques have been used to classify soils and local geology through their geophysical properties, thicknesses, and stratigraphy for more than 25 yr in sensitive and remote environments (e.g., Olson and Doolittle, 1985). Schrott and Sass (2008) reviewed geophysical applications in geomorphology that include determining sediment thickness over bedrock, mapping the thickness of the seasonal permafrost freeze–thaw layer, outlining landslides, sensing seasonal variations in soil fluid content, and quantifying permafrost geophysical properties. Tye et al. (2011) applied multiple geophysical methods with other geologic analyses to describe geologic features in the subsurface. Several studies detail the geophysical methods effective at delimiting permafrost presence and depth of the active layer, as outlined by Kneisel and Hauck (2008).

Streams draining the eastern flank of Colorado's Front Range show evidence of base-level lowering near the range front that has propagated upstream over the past 5 megaannum (Ma) related to changes in climate (Anderson et al., 2006; Wobus et al., 2010). In this predominantly crystalline bedrock setting, the CZ's geology in first-order catchments should be predominantly controlled by the production rates of physical and chemical weathering and the transport of material downslope. We used SSR surveys to characterize the geologic framework of the CZ in the Betasso and Gordon Gulch catchments of the Boulder Creek Critical Zone Observatory (BcCZO), Colorado Front Range, USA (Fig. 2). Although Betasso and Gordon Gulch both drain directly to Boulder Creek, they appear to have significant differences in base-level lowering rates (Schildgen et al., 2002; Anderson et al., 2006): Betasso joins the creek in a deep canyon, suggesting recently increased incision rates, whereas Gordon Gulch joins the creek in a broader canyon upstream of Boulder Creek's knick-point, where incision rates are apparently lower. These differences of base-level lowering histories may be reflected in differences in the geomorphic framework of the CZ and may alter the thickness of the CZ on the hillslopes. Because presently we have only crude models of the evolution of the critical zone in its full architecture, information about the thickness of regolith and about the depth of weathering within the rock mass beneath it will constrain the development of process-based models. For example, if enhanced base-level lowering in Betasso has resulted in a thinning of the CZ, we should see that Gordon Gulch has a thicker mantle of regolith. Also, if stripping material off hillslopes related to base-level lowering has not yet propagated to the broader headwaters of Betasso,

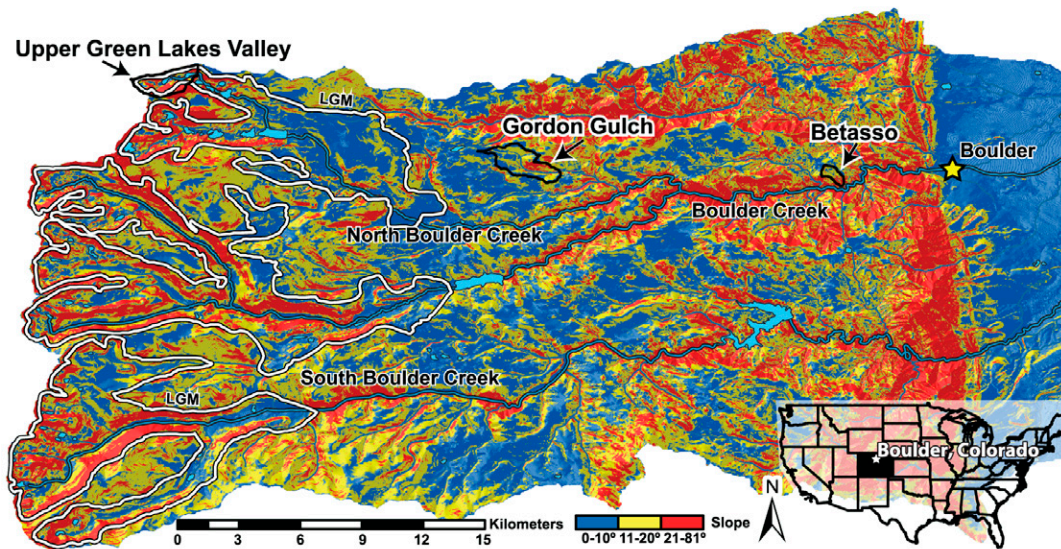


Fig. 2. Three study catchments lie within the mountainous portion of the Boulder Creek Critical Zone Observatory. Each catchment resides within areas with unique recent and ongoing geomorphic processes. Glacially scoured valleys (e.g., upper Green Lakes Valley, and others outlined) lining the continental divide were last occupied during the last glacial maximum (LGM) (Madole et al., 1999). Enhanced river incision moving headward from the range front resulted in steep slopes ($>20^\circ$) along river valleys. Between these geomorphic regimes, the low relief ($<10^\circ$) upland “Rocky Mountain surface” persists with some deeply weathered sections (Dethier and Lazarus, 2006). The Betasso catchment resides on the boundary between heightened river incision and the upland surface. The Gordon Gulch catchment lies completely within the low relief surface.

regolith thickness should increase as a function of distance from the catchment’s outlet. We hypothesize that there is a strong connection between the long-term geomorphic history of a catchment and development of the CZ that in turn reflects the long-term history of the Front Range. We hypothesize that Gordon Gulch should display a deeper and more uniform distribution of weathered bedrock than Betasso. We also hypothesize a transition in the development of the weathered profile in Betasso—thick in the headwaters but truncated near the outlet. This study of the subterranean CZ architecture provides the geologic framework for the active hydrologic, biological, and geochemical processes affecting CZ development and should serve as a guide for future detailed investigations.

Overview of Shallow Seismic Refraction (SSR) and Critical Zone Structure

Shallow seismic refraction techniques use differences in seismic wave speeds, by convention called velocities, of unique subsurface materials (Burger et al., 2006). The density, shear modulus, and bulk modulus of the material together determine the seismic velocity measured by SSR (Telford et al., 1990). Since the subsurface often contains discrete layers (e.g., sediments, regolith, bedrock) with different densities and elastic moduli, seismic wave travel times from a seismic energy source to the sensors (geophones) can be used to recover interface depths and subsurface velocity structure. Seismic energy sources (e.g., sledgehammer in our case) can allow investigations to depths of tens of meters, with depth of penetration also influenced by seismic array geometry and subsurface

properties of the target of investigation (Burger et al., 2006). The resolvability of a single layer depends on its thickness, the contrast in seismic velocity with adjacent layers, and the geophone spacing. Shallow seismic refraction requires increasing seismic velocity of material with depth. “Hidden” layers or other artifacts occur where the velocity contrast is too low or the layer is too thin compared to the sensor spacing, as well as when a low velocity layer underlies a higher velocity layer (Burger et al., 2006). These layers confuse the results and require supplemental data from boreholes or other exposures to guide interpretation.

We employ SSR surveys to determine the compressional or “P” wave velocities (V_p) for distinct materials and their distribution within two catchments of the Boulder Creek watershed. Dense survey networks contribute to the development of a quasi-3D depth to bedrock model for the study areas, where quasi-3D refers to a three-dimensional grouping of two-dimensional surveys for delineating three-dimensional subsurface features. Linkage of stratigraphic, chemical, and physical properties from boreholes and other exposures with SSR surveys can provide estimates of weathering front depths and CZ architecture development on the catchment scale for the full CZ thickness.

In the broadest sense, the subterranean CZ is composed of bedrock with overlying regolith (Fig. 1). Formally, regolith consists of all material above unaltered parent material, crystalline bedrock for this study. The definition of unaltered bedrock depends on the goals, and not just scale, of the study, where physical, chemical,

and mobility boundaries may be assigned between regolith and the parent material (Brantley et al., 2011). We separate regolith into three broad constituents: weathered bedrock, saprolite, and mobile regolith. Bedrock weathering products include soil, grus, saprolite, and oxidized bedrock that may retain original bedrock structures and are unmoved from the original weathering location. Mobile regolith represents any material on the hillslope that has been transported from its original site of weathering and may include soil, alluvium, colluvium, or other transported sediment. Saprolite is rock weathered to the point of being physically weak enough to dig or auger through, but that has not been transported, while weathered rock includes any intact, relatively strong weathered rock. While the seismic signal does travel through soils and mobile regolith, the minimum distance between the sensor and shot (1 m) in this study allows marginal sensitivity to material within 0.5 m of the land surface. Shallow seismic refraction surveys in this study cannot accurately image soils and mobile regolith where they are thinner than 0.5 m. Reducing the geophone spacing may allow imaging of shallower material, but decreases the total survey length and the maximum depth of the investigation. The horizontal and vertical resolutions of SSR results are also related to the geophone spacing, frequencies created by the seismic source, and frequency range measured by the geophones. For this study, the maximum resolution is slightly less than 1 m in the horizontal and vertical directions based on the seismic frequencies recorded. Therefore, both small (<0.5 m) corestones and sparse bedrock fractures could not be imaged.

Estimated P wave velocity (V_p) values for the subsurface interfaces of the model CZ for this study are outlined in Fig. 1. Relatively disaggregated materials generally have low seismic velocity values ($V_p < 700 \text{ m s}^{-1}$) but will be higher if compacted ($V_p > 1000 \text{ m s}^{-1}$); materials with these velocities include mobile regolith, soils, and grus. Unweathered (i.e., intact or jointed) granite and gneiss velocities range from 3500 to 7500 m s^{-1} and are generally $>4000 \text{ m s}^{-1}$ (Barton, 2006; Telford et al., 1990). We estimate saprolite to have a velocity around 1400 m s^{-1} , but in fact it will span the velocity range between disaggregated materials and oxidized bedrock (2000 m s^{-1}). Thus, subsurface layers with intermediate velocities (700–3500 m s^{-1}) represent various grades of weathered crystalline bedrock and compacted weathering products (i.e., sediment, soil, and grus). This classification scheme is consistent with three layer V_p models developed within an alpine environment of the Boulder Creek watershed (Leopold et al., 2008a,b).

Setting

The BcCZO encompasses 1160 km^2 of the Boulder Creek watershed in north-central Colorado and spans 2500 m of elevation from the mountainous headwaters at the continental divide to the High Plains (<http://czo.colorado.edu/>, verified 20 June 2011). The BcCZO spans a broad climate spectrum of both temperature (mean annual temperature of -4°C in the alpine to 11°C in the

plains) and precipitation (mean annual precipitation of 102 cm in the alpine to 46 cm in the plains) (Birkeland et al., 2003). Soils in the Front Range show a strong dependence on the direction the slope faces (slope aspect), with Alfisols on north-facing slopes and Mollisols on south-facing slopes within the cryic temperature regime and ustic moisture regime, overlying mainly oxidized bedrock (Birkeland et al., 2003). Three small catchments sample landscapes characteristic of the mountainous portion of the Boulder Creek watershed as part of the BcCZO (Fig. 2). Anderson et al. (2006) described three geomorphic regimes within the Front Range of Colorado: (i) glacially ornamented valleys along the ridge crest, (ii) a low relief upland “Rocky Mountain surface” (2500–2750 m) that retains deeply weathered profiles up to 15 m thick (Isherwood and Street, 1976; Dethier and Lazarus, 2006), and (iii) catchments bounded by deep bedrock gorges reflecting enhanced river incision near the range front. All carve into Precambrian crystalline bedrock exhumed during the Laramide orogeny (65–45 Ma) of mainly granodiorite (1.7 Ga) and older biotite gneisses (Lovering and Goddard, 1950). Whereas the BcCZO catchments were chosen to represent each of these geomorphic regimes, we focus here on the Betasso and Gordon Gulch catchments.

The Betasso catchment is located 3.2 km upslope from the range front and drains an area of 0.46 km^2 directly into Boulder Creek with an average elevation of 1924 m and vertical range of 240 m. This catchment’s steep, thinly mantled slopes near the confluence with Boulder Creek Canyon reflect the hypothesized high erosional potential caused by the increased river channel incision of Boulder Creek (Anderson et al., 2006). However, further up the catchment, the slopes shallow, with much thicker profiles of weathered bedrock and soil predicted. Ponderosa pine (*Pinus ponderosa* P. Lawson & C. Lawson) forest covers most of Betasso with some small grassy meadows. Immediately adjacent to the Betasso catchment are several other drainages with grassy gentle slopes that shift to pine forest on steeper slopes closer to the bounding stream channels. This transition may mark the contact of the Rocky Mountain surface with the landscape experiencing the effects of the increased channel incision of Boulder Creek. Betasso is underlain by the 1.7 Ga Boulder Creek granodiorite, which outcrops along the ridges and on the steep slopes where the catchment joins Boulder Creek Canyon. A prominent bedrock tor on the western ridge shows the granodiorite to be highly fractured, with generally less than 1.5 m spacing between cracks (E. Dengler, personal communication, 2008). Multiple ravines coalesce, and an ephemeral stream drains the occasional snowmelt out of the catchment through a central gully running northwest to southeast. Some ravines are large and cut down more than 5 m through colluvium to saprolite.

The Gordon Gulch catchment lies within the Rocky Mountain surface and covers an area of 2.7 km^2 . Gordon Gulch has an average elevation of 2716 m and vertical range of 325 m. Gordon Gulch is split into upper and lower sections that both drain west to east with a north–south connection linking them. A dichotomy in

vegetative cover on the slopes strongly reflects this orientation, with dense lodgepole pine (*Pinus contorta* Douglas ex Loudon) forest on the north-facing slopes and sparse ponderosa pine with some grassy undergrowth on the south-facing slopes. Aspen (*Populus tremuloides* Michx.) and shrubs occupy much of the valley floor in the upper catchment. Gordon Gulch therefore represents an excellent study area for determining the effect of aspect on CZ development related to vegetation and catchment structure. The aspen groves in the valley floors accompany marshy conditions with water flowing in the stream year-round. Somewhat inconsistent with the concept of an old slowly eroding upland surface, Gordon Gulch contains steep topography with many bedrock exposures of Precambrian granites, gneisses and schists, especially in the lower portion of the catchment.

Methods

Field Description

For each geophysical line, we used a tape measure, compass, and inclinometer to ensure proper geometry for acquisition and processing. We recorded line descriptions, especially noting vegetation and bedrock outcrop locations. Handheld GPS points mark first and last sensor locations for each individual setup (spread).

Seismic Methods

Shallow seismic refraction surveys were recorded with a 24-channel Geometrics Stratavisor seismograph and twenty-four 40-Hz vertical component geophones. A 5-kg sledgehammer produced the seismic source of energy when striking a 10- by 10- by 7-cm, 15-kg steel plate on the ground surface. Leopold et al. (2008b) calculated that such a source yields vertical blow energy valid for a survey depth range of 2 to 40 m. We used a 2-m geophone spacing resulting in 46-m spread lengths with an approximate 20-m minimum depth of investigation (although this depends on the subsurface velocity structure). Five shots within each spread improved resolution both at shallow depth and for lateral variations along the line, while off-end shots 2 and 5 m from the end geophones provide deeper coverage and expand the total spread length to 56 m (Burger et al., 2006). Multiple spreads generally composed a single line, in which case the final geophone of the previous spread became the first geophone of the next spread, allowing continuity of results across spreads (Fig. 3). At each shot and geophone location, up to 5 cm of organic surficial debris was removed to better couple the shot plate and geophones with the ground surface. Also, three hammer blows secured the plate and compacted additional organic matter or loose sediment to improve the plate's coupling with the ground. Ten hammer blows were stacked at each shot location to reduce uncorrelated noise and increase the amplitude of the seismic signal (Schrott and Sass, 2008).

Seismic data were processed using the SeisImager/2D package (OYO Corporation, 2006). P wave first arrivals were picked automatically and adjusted manually. To capture the subsurface

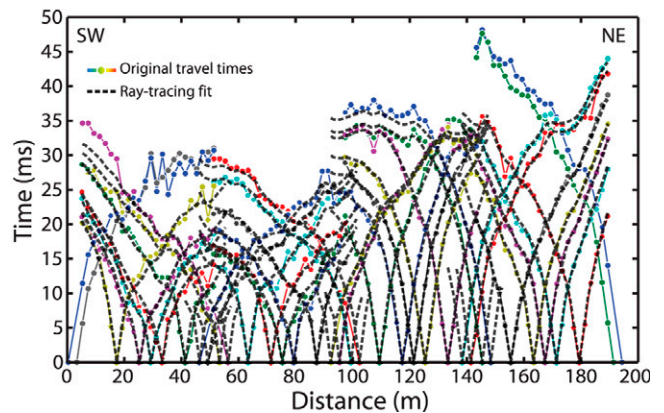


Fig. 3. Seismic travel time plot of P wave first arrivals (colors) for the westernmost Betasso shallow seismic refraction line in Transect 1 (Fig. 5). Steeper slopes of time vs. distance signify slower velocities (slope = velocity⁻¹). A high density of shots per line ensures a more detailed representation of the subsurface in the final velocity profile than the standard three-shot setup (i.e., forward, middle and reverse). The dashed black line represents the calculated travel times from network ray-tracing. RMS misfit = 0.88 ms.

complexities in these mountainous terrains, we employed a travel time tomographic simultaneous iterative reconstruction technique inversion scheme with network ray-tracing in SeisImager/2D (Hayashi and Takahashi, 2001). Time-term inversion and a delay-time reciprocal method were also used in SeisImager/2D to create three layer velocity models that were consistent with the tomographic results but lacked lateral variations within individual layers (Befus, 2010). Tomographic inversion allows lateral heterogeneities that layered inversion schemes cannot represent (Sheehan et al., 2005). In tomographic systems, the cross-section of the subsurface to model is discretized into a grid of cells for both the forward and inverse steps. For our SSR models, all cells were 1 m thick and increased in height from 0.5 m at the surface to 2 m at the lower boundary. The large number of shots per spread ensures dense raypath coverage and more complete sensitivity to the subsurface (Fig. 3). If the observed travel times are longer than the modeled travel times, the modeled raypath travels through higher velocities and/or takes a shorter path in the subsurface than the observed data suggest. Travel time tomography suffers from nonuniqueness associated with inverting geophysical datasets, making reasonable values for the initial model and other inversion parameters essential for recovering the maximum amount of information (Ivanov et al., 2005a,b; Palmer, 2010). We set a standard pseudo-gradient initial model with layers composed of cells of equal velocity that become thicker and increase in velocity with depth and range from 300 m s⁻¹ at the surface to 5000 m s⁻¹ at 10 m depth, where the velocities are standard values for disaggregated material and unweathered crystalline bedrock, respectively (Barton, 2006). Velocity models from the time-term and the reciprocal inversions were also used as initial models for the tomographic inversion with consistent results to the pseudo-gradient initial model (Befus, 2010). Ten iterations of the inversion yielded a root mean square error of less than 3 ms,

on par with the 1- to 3-ms uncertainty associated with manually assigning P wave arrival times. Errors in fitting the travel times with the inverted model will also contribute to a larger root mean square error and can be related to the tomographic discretization. To keep from overfitting the data (i.e., fitting noise in the data), a three-point moving, weighted average of horizontal triplets of cells between inversion steps smoothed lateral differences between cells, where the central cell contributes one-half the smoothed velocity value. No regularization technique was applied within the inversion, only horizontal smoothing between iterations. Raypath coverage provided an estimate of the depth sensitivity and resolution of individual cells in the inverted section, but raypaths are influenced by the selected initial model (Palmer, 2010).

Results

Geophysical data were collected between May and August of 2009. We collected 8.9 km of SSR lines within the two study areas (Fig. 4). Primarily slope-perpendicular transects were selected for SSR surveys where topography and vegetation allowed access in the two catchments. Single SSR lines oriented slope-parallel crossed the larger transects to provide insight into three-dimensional seismic structure of the hillslope.

We purposely avoided exposed bedrock and other rocky terrain due to difficulty in installing geophones. This biases our results toward areas with more regolith overlying bedrock. However, many geophysical lines start near bedrock outcrops to anchor geophysical results to our estimates of local bedrock velocities. Soil pits were dug to refusal in upper Gordon Gulch to a maximum depth of 1.5 m, where saprolite was noted. Multiple boreholes were started in both catchments with a lightweight drill (Shaw Tool Ltd., Yamhill, OR; www.backpackdrill.com/), but loss of engine power from high elevation and the hardness of the weathered crystalline bedrock prevented drilling to depths greater than 2 m. Large boreholes are planned in both catchments to guide future interpretation of the geophysical results.

The product of an SSR inversion is a two-dimensional cross-section of the best-fit subsurface seismic velocity structure based on the inversion parameters and discretization. To describe trends in V_p structure in the catchments, we use two approaches based on the depth to the CZ interface V_p estimates. First, we average the depths to each V_p interface (contoured from the gridded inversion output) for all SSR lines in a catchment and calculate the standard deviation for the whole catchment. Second, we calculate the average depth to each interface across individual SSR lines, noting the line-specific standard deviations. Considering individual lines allows the separation of differences between opposing hillslopes and locations within the catchments.

Results from Betasso Catchment

A total of 4.5 km of SSR surveys were conducted in the Betasso catchment. Three main transects of SSR lines cross the Betasso catchment toward the headwaters, center, and mouth of the drainage area (Fig. 5). Continuous lines were not possible because of a steep gully running down the center of the catchment, smaller ravines, and roads.

Figures 6 and 7 provide an overview of SSR results in Betasso across the whole catchment and by consolidating individual line results, respectively. Shallow seismic refraction profiles in Betasso located the line-average depth of high velocity material ($V_p > 3500 \text{ m s}^{-1}$) at 7.2 to 15.0 m depth, with all the data marking this interface at $12 \pm 2.8 \text{ m}$ depth. In general, intermediate velocity material ($2000 \text{ m s}^{-1} < V_p < 3500 \text{ m s}^{-1}$) appeared closer to the surface further upslope from the valley center, with a catchment-average depth of $6.0 \pm 2.4 \text{ m}$. Slightly lower velocity material ($V_p = 1400 \text{ m s}^{-1}$) appeared at average depths of 1.3 to 7.3 m per line, and $3.4 \pm 1.8 \text{ m}$ over the whole catchment. The lowest velocity materials ($V_p < 700 \text{ m s}^{-1}$) were found to average depths of 0.3 to 3.3 m of each SSR line, but extended to 5 m depth toward the top of the catchment. Overall in Betasso, 700 m s^{-1} was found at $0.94 \pm 0.8 \text{ m}$ depth and is in most places shallower than the SSR survey's sensitivity for the 2 m geophone spacing we employed.

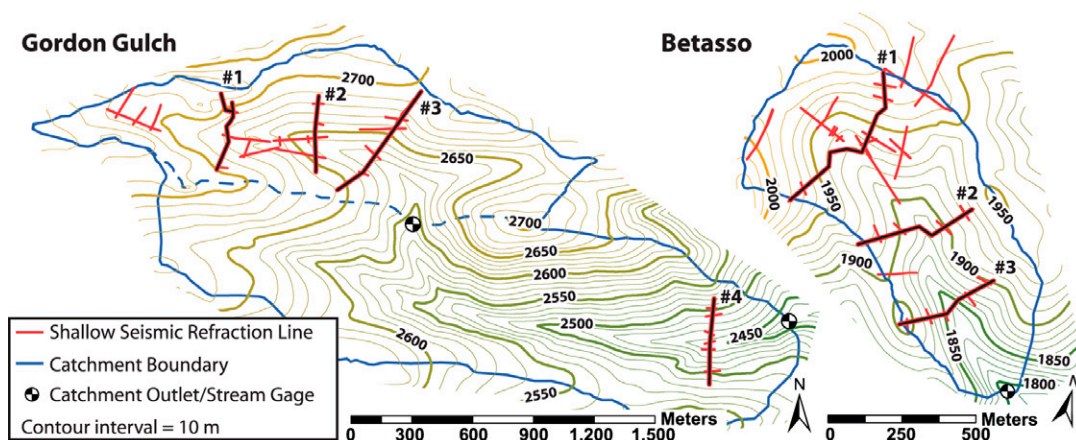


Fig. 4. Overview of shallow seismic refraction (SSR) lines collected May through August 2009. Numbered black lines show transect locations for Fig. 5 and 8. Note different scales and slight changes in orientation.

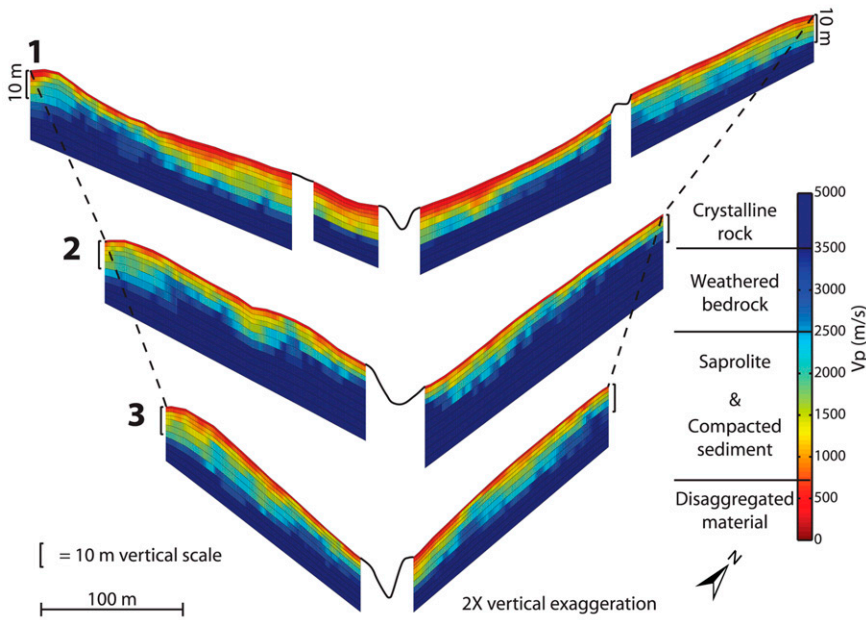


Fig. 5. Three shallow seismic refraction transects through the Betasso catchment with locations shown in Fig. 4. Low velocity (red) values are thick in the upper transect but are thinner in the lower two transects.

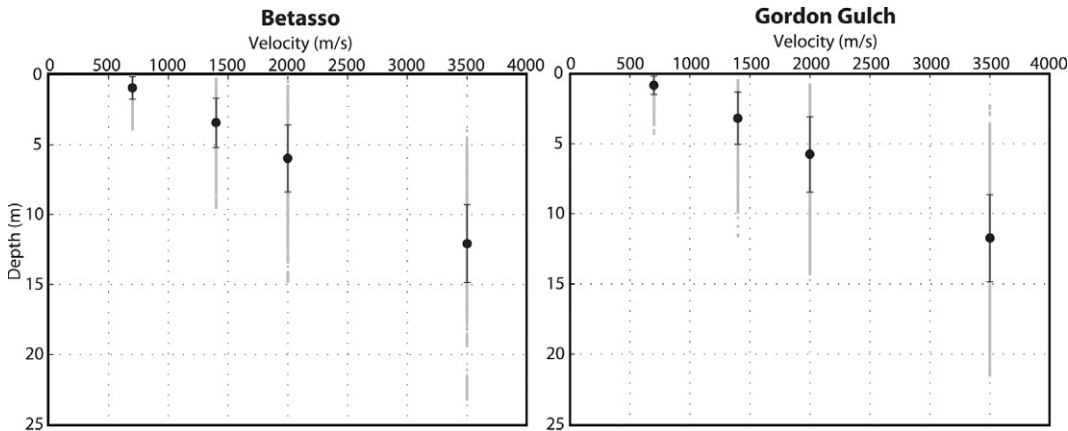


Fig. 6. Summary of all shallow seismic refraction lines in both catchments. Each value was computed from all the data points within each catchment marked by the depth of the velocity value, where n refers to the number of velocity data points used to compute the statistics.

Depth to velocity value from surface (m)

	700 m/s	1400 m/s	2000 m/s	3500 m/s
Maximum	3.9	9.5	14.8	23.2
Minimum	0.0	0.3	0.0	1.5
Mean	0.9	3.4	6.0	12.1
Std Dev	0.8	1.8	2.4	2.8
	n=3837	n=3853	n=4049	n=4135

Depth to velocity value from surface (m)

	700 m/s	1400 m/s	2000 m/s	3500 m/s
Maximum	4.3	11.6	14.3	21.5
Minimum	0.0	0.5	0.8	2.3
Mean	0.9	3.2	5.8	11.7
Std Dev	0.7	1.9	2.7	3.1
	n=4266	n=4492	n=4488	n=4309

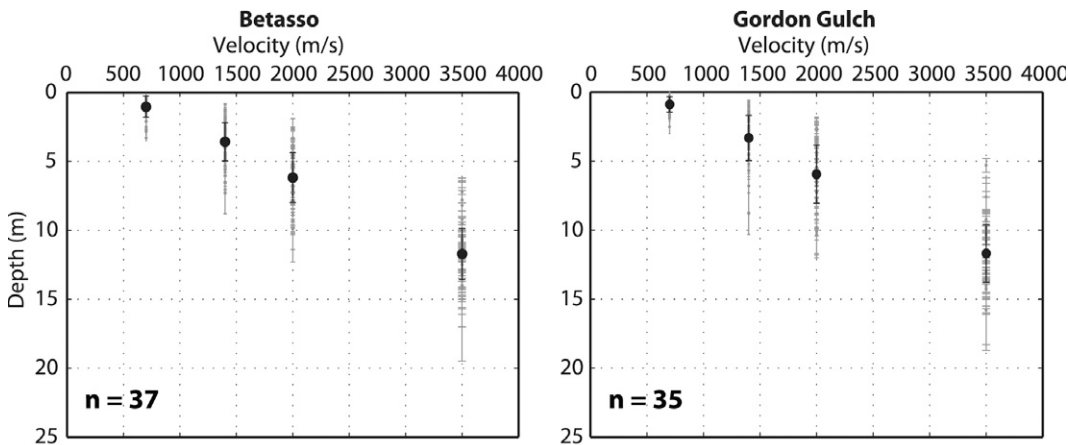


Fig. 7. Summary of catchment line averages. Depths to the velocity values for individual lines were first averaged, and then these line-averages statistics were found, where n refers to the number of lines in each catchment. Line-average results reveal variability related to line location or local weathering features. Mean line statistics show overall shallow seismic refraction line trends in the catchments.

Mean depth to velocity value from surface (m)

	700 m/s	1400 m/s	2000 m/s	3500 m/s
Maximum	3.3 ± 0.2	7.3 ± 1.5	9.9 ± 1.5	15.0 ± 4.5
Minimum	0.3 ± 0.1	1.3 ± 0.5	2.6 ± 0.7	7.2 ± 0.8
Mean	1.0 ± 0.8	3.6 ± 1.4	6.2 ± 1.8	11.7 ± 1.8

Mean depth to velocity value from surface (m)

	700 m/s	1400 m/s	2000 m/s	3500 m/s
Maximum	2.5 ± 0.5	8.8 ± 1.5	10.3 ± 1.5	15.8 ± 2.9
Minimum	0.3 ± 0.1	1.0 ± 0.3	2.6 ± 0.8	5.3 ± 0.5
Mean	0.9 ± 0.5	3.3 ± 1.6	5.9 ± 2.1	11.7 ± 2.1

The three SSR transects across Betasso reveal the V_p structure of the upper 20 m of the hillslopes with increasing distance from the catchment mouth. The uppermost transect (#1) marks high velocities ($V_p > 3500 \text{ m s}^{-1}$) mainly at depths of 12 m deep with short convexities ($<10 \text{ m}$) where the interface shallows to depths of 8 m. Intermediate velocities ($V_p = 1400 \text{ m s}^{-1}$) are found at depths no deeper than 7 m. Low velocity values ($V_p < 700 \text{ m s}^{-1}$) range from 1 m up to 5 m depth. These thicken toward the valley center. In the upper transect SSR profiles showed less than 2 m of low velocity materials in general, although these materials lie in the poorly constrained portion of the model. Intermediate velocity values extended no deeper than 5 m in the middle transect. High velocity materials were found at depths that shallowed downslope but remained mostly constant at 8 to 10 m depth. Moderately high velocity ($>2000 \text{ m s}^{-1}$) knobs in the middle transect approached the surface. In the lowest transect, less than 2 m of low velocity material were present in the profiles. Intermediate values ranged between depths of 2 and 7 m. High velocity values were modeled mainly 8 m from the surface but reached depths of 17 m near the western ridge crest.

From the upper to middle transects, the low and intermediate velocity interfaces appeared to shallow. A valley-center SSR line between these two transects revealed a shallowing of the high velocity interface 50 m down-catchment from the upper transect, from 12 to 4 m depth. For the middle and lower transects, the principal gradients in interface depths appeared to be along contour rather than up- and downslope.

Gordon Gulch Results

A total of 4.4 km of SSR surveys were conducted in the Gordon Gulch catchment, concentrated in the upper half of the drainage. Four sets of SSR lines ran across the drainage, three in the upper portion and one in the lower drainage (Fig. 8). Low relief in the upper catchment allowed continuous transects across the catchment.

Figures 6 and 7 provide an overview of SSR results in Gordon Gulch. Across the 35 SSR lines in Gordon Gulch, line-average depths to high and intermediate material were 5.3 to 15.8 and 1.0 to 8.8 m, respectively. Moderately high velocities ($>2000 \text{ m s}^{-1}$) were encountered at depths of $5.8 \pm 2.7 \text{ m}$, and line-averages ranged between 2.6 and 10.3 m. Overall, high velocity (presumably unweathered) materials were imaged at $11.7 \pm 3.1 \text{ m}$ depth. Intermediate velocity materials were found at an average $3.2 \pm 1.9 \text{ m}$ depth in the catchment. The lowest velocity materials varied between line-averages

of 0.3 and 2.5 m thick and $0.9 \pm 0.7 \text{ m}$ thick for the catchment. Intermediate velocities were encountered to greater depths on the southern slope (10.9–15.3 m) compared to both the valley center (8.4–11.9 m) and northern slope (10.9–12.9 m).

The four transects in Gordon Gulch revealed a transition from uniform deep high velocities in the uppermost portion to a consistent difference between deeper high velocities on the southern slopes and shallower high velocities on the northern slopes. In the uppermost transect (#1), high velocity materials were imaged at 15 m depth across the catchment with $<2 \text{ m}$ of low velocity material. Intermediate velocity material ranged from 2 to 4 m deep on both slopes, with a 60-m-wide, high velocity mound on the southern slope. The second transect crossed through an open meadow 400 m up-drainage, where high velocity values on the southern slope appeared at 19 m depth. In the central valley these velocities occur at a depth of 13 m and shallow to 8 m for most of the northern slope, and are interrupted by a 50-m-long deepening to 15 m depth. Intermediate velocity material spanned from 4 to 6 m depth on the southern slope and was thinner ($\sim 2 \text{ m}$) on the northern slope. Low velocity material reached a maximum thickness of 2 m under the central meadow but was generally $<1 \text{ m}$ thick.

The third transect was the lowest in upper Gordon Gulch, 300 m down-drainage from the second transect. The northern slope had thin low velocity material ($<1 \text{ m}$) with 1400 m s^{-1} at 4 m depth. High velocity values were imaged at 10 m depth with a broad 75

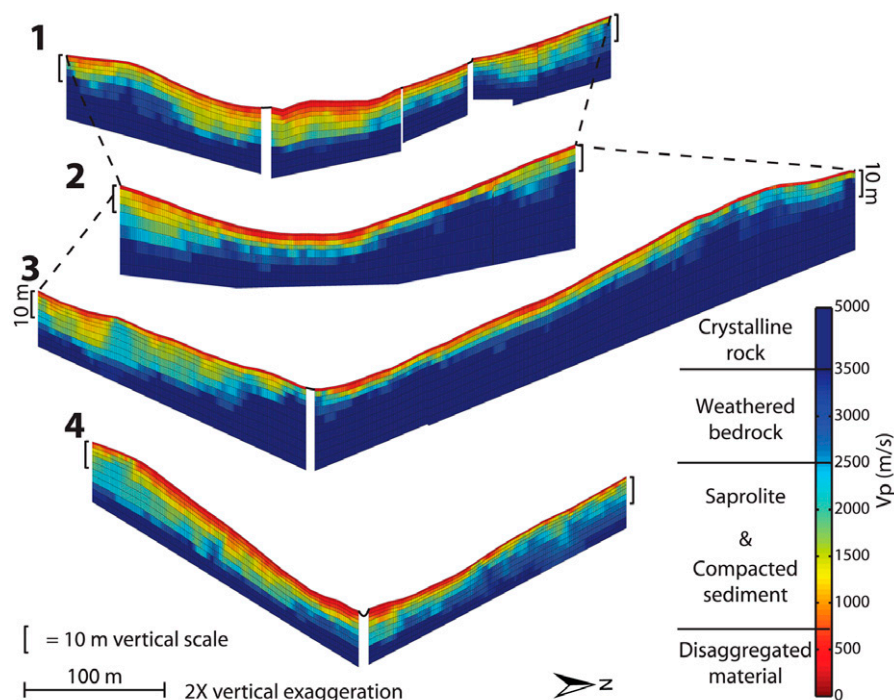


Fig. 8. Four shallow seismic refraction transects across the Gordon Gulch catchment with locations shown in Fig. 4. North-facing slopes show consistently deeper low velocities ($<2500 \text{ m s}^{-1}$) and likely describe deeper weathering fronts compared to the profiles on the south-facing slope.

m knob of material $> 2000 \text{ m s}^{-1}$ that reached to within 4 m of the surface. In the valley center, high velocity values were imaged within 5 m of the ground surface but deepened to 16 m along the southern slope. Intermediate velocity materials on the southern slope remained 2 m from the surface, except in pockets deepening the interface to a maximum 8 m depth. Low velocity material was $< 1 \text{ m}$ thick. The final transect (#4) ran 500 m from the outlet of the Gordon Gulch watershed. On the northern (south-facing) slope, SSR imaged 3500 m s^{-1} and greater velocities at 14 m depth, with moderate velocities $> 2000 \text{ m s}^{-1}$ reaching to within 3 m of the ground surface. The SSR transect showed abundant intermediate velocity values at 5 to 7 m depth, but these materials were at 3 m depth for the majority of the line. The southern (north-facing) slope profile showed high velocity values at 19 m depth that shallowed to 13 m near the valley center. Low velocity material was generally 3 m thick but less than 1 m toward the top of the southern slope. The northern (south-facing) slope SSR lines revealed fast velocities at consistently shallower depths than on the southern (north-facing) slope for the lower three transects (#2–4).

Discussion

The SSR lines cover a large portion of two catchments studied in the BcCZO, documenting the V_p structure of the subsurface. The classification scheme outlined in Fig. 1 was applied to both catchments, allowing quasi-3D subsurface geologic interpretation of SSR profiles (Fig. 9). Generally, unweathered bedrock appeared within 20 m of the ground surface. Even so, the CZ may extend beyond our definition of fresh bedrock, as joints and fractures could provide water pathways where biological and chemical processes advance the weathering process. Bedrock geology varies across the catchments, and includes granodiorite, schist, and gneiss that could introduce complexity in interpreting the depth to fresh bedrock. However, as both fresh and weathered V_p values for these

rock types are nearly identical (Barton, 2006), we expect that this variability of bedrock type does not dominate the signals we have documented.

The shallowing of fresh bedrock between the upper (#1) and middle (#2) transects in Betasso suggests that the transient signal of enhanced erosion associated with a lowering in base level has not reached the upper transect: thicker disaggregated material ($1.33 \pm 0.8 \text{ m}$) and saprolite ($4.0 \pm 1.4 \text{ m}$) remain high in the catchment compared to below transect 2 (0.6 ± 0.2 and $2.9 \pm 1.0 \text{ m}$, respectively). These data suggest increased sediment stability, which is supported by ravine exposures with 4 m of layers of sediment, a paleosol, and new soils dating back to 18 ka above the uppermost SSR transect (Leopold et al., 2011). Alternatively, the upper transect represents a snapshot of the subsurface where the signal of increased transport could be active but only for a short period of time. Thus, the effect of the rejuvenated incision of Boulder Creek appears to extend a maximum of 1000 m up the Betasso drainage basin, but no less than 500 m.

The SSR lines on the western slope show slightly deeper weathering than those on the eastern slopes in the lower portion of the catchment. Aspect-related conditions provide a plausible explanation, as the western slope faces northeast and is shadowed more often than the eastern slope. This could lead to less evaporation and more water availability for weathering processes in the subsurface. Even with weathering visible in the SSR profiles, the majority of weathering products in Betasso are efficiently transported downslope to the valley center, where they either reside unaffected by the fluvial incision or are flushed out of the catchment.

Perhaps the largest signal in Gordon Gulch is associated with the aspect of the slope. Differences between the north- and south-facing slope V_p structure in Gordon Gulch may result from either different

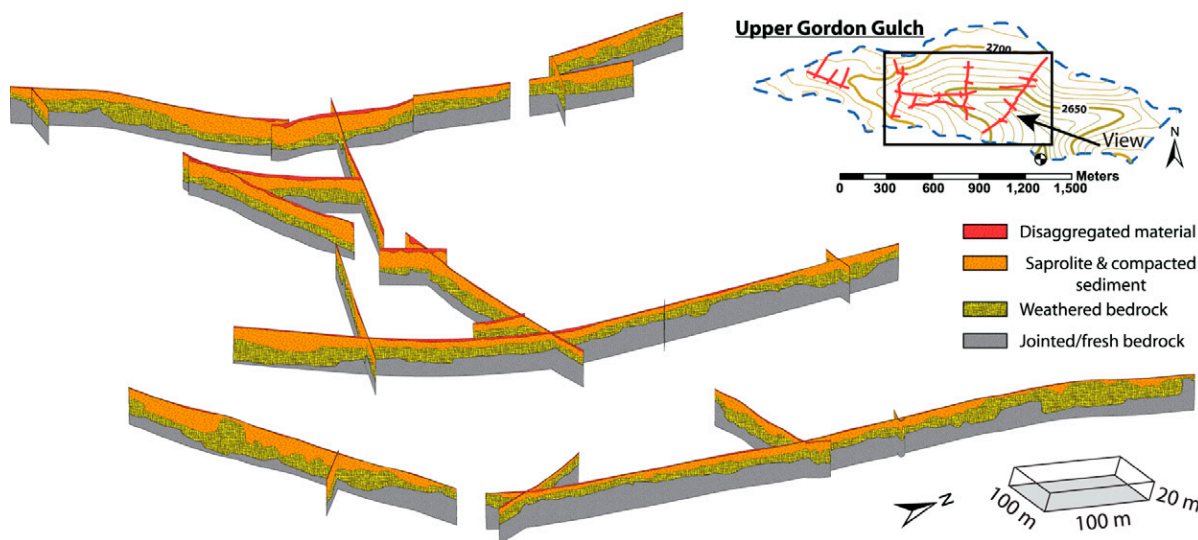


Fig. 9. Velocity assignments for geologic materials yield a quasi-3D network of interpreted critical zone architecture. Select shallow seismic refraction lines from the upper Gordon Gulch catchment reveal subsurface structure over 0.5 km^2 to a depth of 20 m.

susceptibilities of the substrate to weathering or a difference in weathering rates. Within the low relief upper Gordon Gulch, interpreted weathering to 20 m depth and the buildup of more than 4 m of disaggregated material in the valley center may mean this area is transport-limited. Lower in the catchment the north-facing slope consistently displayed much deeper weathering (1400 m s^{-1} at $4.2 \pm 1.4 \text{ m}$ and 2000 m s^{-1} at $8.1 \pm 1.5 \text{ m}$ depth) than the south-facing slope (1400 m s^{-1} at $1.9 \pm 0.5 \text{ m}$ and 2000 m s^{-1} at $3.8 \pm 1.0 \text{ m}$ depth). Weathered bedrock values ($2000 \text{ m s}^{-1} < V_p < 3500 \text{ m s}^{-1}$) extended to depths greater than 10 m on the north-facing slope, but to depths of 5 to 7 m at the valley floor and on the south-facing slope. In the lower drainage of Gordon Gulch, a similar pattern showed weathered bedrock velocities beyond 15 m depth on the southern (north-facing) slope and 5 to 10 m on the northern (south-facing) slope. This difference in depth of weathering may reflect greater moisture retention of the north-facing slope that is promoted by denser vegetation cover and longer lasting snowpacks. On the other hand, higher erosion rates on the south-facing slope would efficiently remove weathering products and yield similar results. If south-facing slopes were steeper, this would explain such efficient removal of detritus; however, SSR lines were collected where valley slopes were similar (see Fig. 4 and 8). Alternatively, Pleistocene periglacial activity, such as solifluction, may explain shallower bedrock on the less shadowed south-facing slope, where higher solar radiation allows more intense periglacial activity, as weathering products would be more efficiently transported downslope during the summer (Raab et al., 2007). Evidence of periglacial activity is present in multilayered slope debris sections near Gordon Gulch (Völkel et al., 2011). While we cannot discriminate between these alternative interpretations with shallow geophysics alone, the CZ architecture we have revealed strongly constrains models of hillslope and CZ development.

If Betasso and Gordon Gulch are catchments with weathering patterns that are characteristic of the regional erosional regimes, the interpreted geologic framework of the CZ in each catchment can be compared with regional studies of CZ structure in those regimes. Using an areally extensive array of well logs, Dethier and Lazarus (2006) documented a mean highly weathered regolith thickness of 3.3 m, and a mean depth to fresh bedrock of 7 m depth in the low relief Rocky Mountain surface. These match well with the valley floor and south-facing slope velocity profiles in Gordon Gulch, but not the deeper weathering on north-facing slopes suggested by the SSR results. However, the data of Dethier and Lazarus (2006) may not capture the bimodal pattern of weathering related to aspect suggested by the velocity models as they reside mainly on south-facing slopes and in valleys. Dethier and Lazarus (2006) did mention large local areas of weathered regolith thickness exceeding 10 m, but provided no information about aspect. Even so, the geophysical lines were laid out to avoid bedrock outcrops and very rough terrain that complicate or prevent the insertion of geophones. This bias likely results in an overestimation of the thickness of the weathered zone above bedrock.

Both Betasso and Gordon Gulch contain weathering fronts that extend to an average depth of about 12 m, assuming our assignment of fresh bedrock is correct. This result is not consistent with our working hypothesis where Gordon Gulch would contain deeper sections of weathered material and more advanced weathering fronts than found in Betasso. Shallow seismic refraction results in Betasso set the mean depth to each subsurface interface consistently, though marginally, deeper than in Gordon Gulch (Fig. 6). However, the observation of greater regolith thicknesses high in the Betasso catchment and the strong contrast in depth of weathering of north- and south-facing slopes in Gordon Gulch complicate these results. Thus, we cannot reject the possibility of deeper weathered sections over the low relief upland surface compared to areas under the influence of enhanced Boulder Creek channel incision.

Layered velocity models, rather than tomographic models, continue to be the standard method of interpreting SSR data, requiring only an interpretation of predominantly vertical velocity transitions (e.g., Leopold et al., 2008a,b; Schrott and Sass, 2008; Travelletti et al., 2010). Layered velocity models can be constructed with fewer shot locations that reduce acquisition time, where SSR tomography needs dense shot locations to ensure raypath coverage within the modeled area. This tomographic inversion method also applies a velocity gradient whether or not one exists in reality, making interpretation more difficult (Sheehan et al., 2005). A constant-value initial model with little regularization could return a rough or blocky inversion output that may or may not have real world significance. However, tomographic inversion captures horizontal and vertical velocity heterogeneities that may prove critical where true velocity gradients exist in the subsurface, as is the case in weathered profiles. In this case, high vertical velocity gradients would mark discrete interfaces that may transform into a low velocity gradient, smooth weathered profile along the same line (Fig. 10). Layered velocity models from time-term and reciprocal method inversions showed consistent, broad velocity structures in the tomographic results without capturing any lateral heterogeneity within layers (Befus, 2010).

Other Methods

Multiple geophysical methods applied to the same location can provide complementary datasets for outlining subterranean structure (Schrott and Sass, 2008). Ground-penetrating radar (GPR) utilizes the reflection of high frequency (1–1000 MHz) electromagnetic waves to obtain a detailed image of subsurface interfaces. Scattered GPR reconnaissance lines were collected and support our SSR results (Leopold et al., 2009). Electrical resistivity tomography (ERT) surveys employ multi-electrode configurations to probe the electrical resistivity structure of the subsurface and are very sensitive to water and clay content. We collected 2.75 km of ERT surveys mainly in the Betasso catchment (Leopold et al., 2009). These data lack information on some subsurface structure gained from the SSR surveys in Betasso for two reasons. First, the data

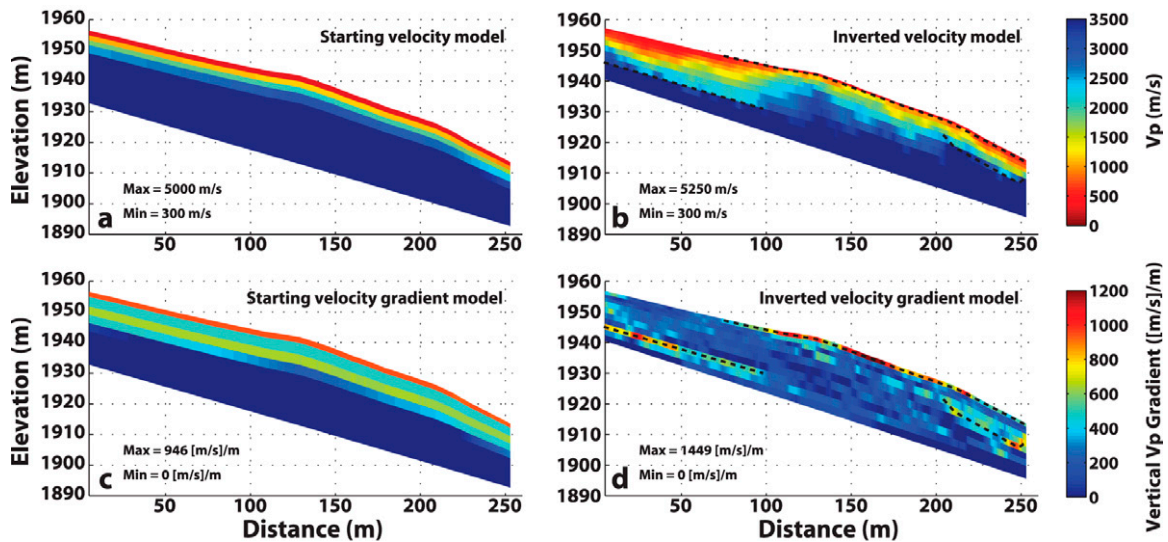


Fig. 10. Vertical velocity gradient models (c and d) reveal discrete interfaces (high gradient) and smooth gradations (low gradient) in subsurface material properties. Initial model parameters (a and c) influence the inverted profiles but are guided by the inversion toward a subsurface velocity model (b and d) that minimizes the misfit of the model with the data (RMS misfit = 0.66 ms). Dashed lines emphasize high vertical gradients where discrete geological interfaces are most likely.

were collected during a very rainy period and may capture areas of increased water content that mask the subsurface resistivity structure. Second, many of the surveys in Betasso cross or pass very close to buried steel pipes that create artifacts and confuse the inverted profiles. However, ERT lines in Gordon Gulch show equivalent subsurface structures when compared with SSR profiles (Leopold et al., 2009). Seismic reflection surveys would provide data that are similar to GPR but require sufficient seismic velocity contrasts that are often absent in undisturbed weathered profiles. Few discernable reflections were visible in our data associated with velocity interfaces.

Shallow seismic refraction surveys capture the subterranean spectrum of weathering across each study area. The initial phases of in situ bedrock weathering are inherently difficult to study when fresh bedrock lies well below the land surface and is rarely the target. However, dynamic landscapes, such as those in the Boulder Creek watershed, require a firm understanding of both surficial and subterranean processes that may tend to stabilize or weaken individual landscape parcels and hillslopes. The quasi-3D framework of SSR lines begins to describe trends in the weathering front development and the thickness of disaggregated materials. Boreholes and other excavations guided by the SSR results can be used to sample the weathering signature of the physical, chemical, and biological processes that shape the CZ at the most informative locations and provide critical information on the true geologic framework that will allow more quantitative interpretation of the geophysical results. If these processes leave distinct enough geophysical footprints, measuring their three-dimensional extent to understand their distributions in a catchment would no longer require an expensive network of

boreholes. Instead, measurements from well-sited boreholes and other excavations should guide the interpretation of geophysical surveys in the context of those processes, especially in difficult drilling environments.

Conclusions

The CZ represents the life-sustaining realm of the terrestrial surface. As such, the processes that control the development and consequent transformation of the CZ are important to the continued health of the planet as the breadth of human influences on the system continues to grow. A first-order requirement for understanding the CZ is knowledge of the geologic framework of the subsurface. This subterranean structure reflects the operation of both modern and past processes. We employed shallow seismic refraction to detect the V_p distribution in the subsurface with minimal disruption of either the materials or the operative processes. In addition, SSR covers large areas in less time and at less expense than measurements from boreholes or deep soil pits. Such labor-intensive measurements nonetheless provide ground truth and critical constraints for interpreting the geophysical results.

Shallow seismic refraction surveys throughout two catchments within the Boulder Creek watershed capture snapshots of the subsurface architecture that are relevant to the understanding of weathering and transport processes. Characteristic P wave velocities were estimated for disaggregated materials ($<700 \text{ m s}^{-1}$), saprolite and compacted sediment ($700\text{--}2000 \text{ m s}^{-1}$), weathered bedrock ($2000\text{--}3500 \text{ m s}^{-1}$), and crystalline bedrock ($>3500 \text{ m s}^{-1}$). We used networks of SSR profiles to construct quasi-3D

networks (fence diagrams) of CZ architecture and the depth to bedrock in each field area.

Geophysical profiles in the Betasso catchment suggest a break in the overburden thickness that fits the broader geomorphic context (i.e., upward carving fluvial incision) of the catchment within the Boulder Creek watershed. Interpreted SSR lines show a break to relatively thin sections of disaggregated materials within 1000 to 500 m of the catchment outlet. In contrast, deep weathering to depths of 23 m occurs throughout the remainder of Betasso and displays a pattern suggesting that bedrock is nearer the surface further upslope from the center of the catchment. On average across the catchment, P wave velocities corresponding to fresh bedrock appeared at a depth of 12.1 ± 2.8 m. Geophysical surveys and carefully chosen excavations guided by these results can now be applied to constrain more tightly the apparent progression of an erosional wave upward into the catchment.

Geophysical results in the Gordon Gulch catchment displayed deep (>15 m) and extensive weathered profiles, supporting the hypothesis that the CZ here reflects the subsurface expression of a broad low relief upland Rocky Mountain surface. Weathering front advance in Gordon Gulch is dependent on slope aspect, especially on steep slopes. Across the catchment, bedrock appeared at an average depth of 11.7 ± 3.1 m. Shallow slopes toward the top of Gordon Gulch also display thick disaggregated materials (4 m) and deep weathering (>15 m).

The results from these two subcatchments reveal subsurface snapshots of a well-developed CZ in a landscape sculpted by dynamic and connected geomorphic processes. Overall, Betasso and Gordon Gulch display similar mean interface depths, suggesting similarity in the weathering process rates and the time over which these processes have been active. The Betasso site spans the boundary between the low relief upland surface and the ongoing incision of Boulder Creek at its catchment exit. In detail, the SSR lines reveal complexities within both catchments related to aspect and catchment geometry that together inspire and provide quantitative constraint on process-related research in the Boulder Creek watershed aimed at understanding the breakdown and exhumation of bedrock.

Acknowledgments

We thank G. McClave, K. Anarde, A. Andrus, D. Culp, and T. Kelsay for their help in the field and the University of Colorado Geological Sciences Mentorship program and the IRIS Undergraduate Internship Program for support of the undergraduate field assistants. IRIS PASSCAL provided equipment for part of the SSR experiment, and Bill Stephenson from the USGS kindly loaned us geophones. Thoughtful comments from two anonymous reviewers helped improve the manuscript. This work was supported by National Science Foundation Grant NSF-EAR 0724960, which established the Boulder Creek Critical Zone Observatory.

References

Anderson, R.S., C.A. Riihimaki, E.B. Safran, and K.R. MacGregor. 2006. Facing reality; late Cenozoic evolution of smooth peaks, glacially or-

namented valleys, and deep river gorges of Colorado's Front Range; Tectonics, climate, and landscape evolution. *Spec. Pap. Geol. Soc. Am.* 398:397–418.

Anderson, S.P., F. von Blanckenburg, and A.F. White. 2007. Physical and chemical controls on the critical zone. *Elements* 3:315–319. doi:10.2113/gselements.3.5.315.

Barton, N. 2006. Rock quality, seismic velocity, attenuation and anisotropy. Taylor and Francis Group, London.

Befus, K.M. 2010. Applied geophysical characterization of the shallow subsurface: Towards quantifying recent landscape evolution and current processes in the Boulder Creek watershed, CO. M.S. thesis. University of Colorado, Boulder.

Birkeland, P.W., R.R. Shroba, S.F. Burns, A.B. Price, and P.J. Tonkin. 2003. Integrating soils and geomorphology in mountains—an example from the Front Range of Colorado. *Geomorphology* 55:329–344. doi:10.1016/S0169-555X(03)00148-X.

Brantley, S.L., M.B. Goldhaber, and K.V. Ragnarsdottir. 2007. Crossing disciplines and scales to understand the critical zone. *Elements* 3:307–314. doi:10.2113/gselements.3.5.307.

Brantley, S.L., J.P. Megonigal, F.N. Scatena, Z. Balogh-Brunstad, R.T. Barnes, M.A. Bruns, P. Van Cappellen, K. Dontsova, H.E. Hartnett, A.S. Hartshorn, A. Heimsath, E. Herndon, L. Jin, C.K. Keller, J.R. Leake, W.H. McDowell, F.C. Meinzer, T.J. Mozdzer, S. Petsch, J. Pett-Ridge, K.S. Pregitzer, P.A. Raymond, C.S. Riebe, K. Shumaker, A. Sutton-Grier, R. Walter, and K. Yoo. 2011. Twelve testable hypotheses on the geobiology of weathering. *Geobiology* 9(2):140–165 doi:10.1111/j.1472-4669.2010.00264.x.

Burger, H.R., A.F. Sheehan, and C.H. Jones. 2006. Introduction to applied geophysics: Exploring the shallow subsurface. W.W. Norton, New York.

Dethier, D.P., and E.D. Lazarus. 2006. Geomorphic inferences from regolith thickness, chemical denudation and CRN erosion rates near the glacial limit, Boulder Creek catchment and vicinity, Colorado. *Geomorphology* 75:384–399. doi:10.1016/j.geomorph.2005.07.029.

Egli, M., A. Mirabella, G. Sartori, R. Zanelli, and S. Bischof. 2006. Effect of north and south exposure on weathering rates and clay mineral formation in Alpine soils. *Catena* 67:155–174. doi:10.1016/j.catena.2006.02.010.

Hayashi, K., and T. Takahashi. 2001. High resolution seismic refraction method using surface and borehole data for site characterization of rocks. *Int. J. Rock Mech. Min. Sci.* 38:807–813. doi:10.1016/S1365-1609(01)00045-4

Isherwood, D., and A. Street. 1976. Biotite-induced grussification of the Boulder Creek Granodiorite, Boulder County, Colorado. *Geol. Soc. Am. Bull.* 87:366–370. doi:10.1130/0016-7606(1976)87<366:BGOTBC>2.0.CO;2.

Ivanov, J., R.D. Miller, J. Xia, D. Steeples, and C.B. Park. 2005a. The inverse problem of Refraction travel times, part I: Types of geophysical nonuniqueness through minimization. *Pure Appl. Geophys.* 162:447–459. doi:10.1007/s00024-004-2615-1.

Ivanov, J., R.D. Miller, J. Xia, and D. Steeples. 2005b. The inverse problem of refraction travel times, Part II: Quantifying refraction nonuniqueness using a three-layer model. *Pure Appl. Geophys.* 162:461–477. doi:10.1007/s00024-004-2616-0.

Jin, L., R. Ravella, B. Ketchum, P.R. Bierman, P. Heaney, T. White, and S.L. Brantley. 2010. Mineral weathering and elemental transport during hillslope evolution at the Susquehanna Shale Hills Critical Zone Observatory. *Geochim. Cosmochim. Acta* 74:3669–3691. doi:10.1016/j.gca.2010.03.036.

Kneisel, C., and C. Hauck. 2008. Applied geophysics in periglacial environments. Cambridge Univ. Press, Cambridge.

Leopold, M., D. Dethier, J. Völkel, and T. Raab. 2008a. Combining sediment analysis and seismic refraction to describe the structure, thickness and distribution of periglacial slope deposits at Niwot Ridge, Rocky Mountains Front Range, Colorado, USA. *Z. Geomorphol. Suppl.* 52:77–94. doi:10.1127/0372-8854/2008/0052S2-0077.

Leopold, M., D. Dethier, J. Völkel, T. Raab, T.C. Rikert, and N. Caine. 2008b. Using geophysical methods to study the shallow subsurface of a sensitive alpine environment, Niwot Ridge, Colorado Front Range, USA. *Arct. Alp. Res.* 40:519–530. doi:10.1657/1523-0430(06-124)[LEOPOLD]2.0.CO;2.

Leopold, M., J. Völkel, and D. Dethier. 2009. Imaging the Critical Zone using ground penetrating radar and electric resistivity. Initial results from the Boulder Creek Critical Zone Observatory. *Geophys. Res. Abstr.* 11:EGU2009–EGU9450.

Leopold, M., J. Völkel, D. Dethier, J. Huber, and M. Steffens. 2011. Characteristics of a paleosol and its implication for the Critical Zone development, Rocky Mountain Front Range of Colorado, USA. *Appl. Geochem.* 26(Suppl. 1):S72–S75, doi:10.1016/j.apgeochem.2011.03.034

Lovering, T.S., and E.N. Goddard. 1950. Geology and ore deposits of the Front Range, Colorado. USGS Prof. Paper 223.

Madole, R.F., D.P. VanSistine, and J.A. Michael. 1999. Pleistocene glaciation in the upper Platte River drainage basin, Colorado. *USGS Geol. Invest. Ser. I-2644.*

- Olson, C.G., and J.A. Doolittle. 1985. Geophysical techniques for reconnaissance investigations of soils and surficial deposits in mountainous terrain. *Soil Sci. Soc. Am. J.* 49:1490–1498. doi:10.2136/sssaj1985.03615995004900060032x.
- OYO Corporation. 2006. SeisImager/2D manual, Ver. 3.2. Available at ftp://geom.geometrics.com/pub/seismic/SeisImager/Installation_CD/SeisImager2D_Manual/ (verified 20 June 2011).
- Palmer, D. 2010. Non-uniqueness with refraction inversion—a syncline model study. *Geophys. Prospect.* 58:203–218. doi:10.1111/j.1365-2478.2009.00818.x.
- Raab, T., M. Leopold, and J. Völkel. 2007. Character, age, and ecological significance of Pleistocene periglacial slope deposits in Germany. *Phys. Geogr.* 28:451–473. doi:10.2747/0272-3646.28.6.451
- Rossi, A.M., and R.C. Graham. 2010. Weathering and porosity formation in subsoil granitic clasts, Bishop Creek Moraines, California. *Soil Sci. Soc. Am. J.* 74:172–185. doi:10.2136/sssaj2009.0146
- Schildgen, T., D.P. Dethier, P. Bierman, and M. Caffee. 2002. ²⁶Al and ¹⁰Be dating of late pleistocene and holocene fill terraces: A record of fluvial deposition and incision, Colorado front range. *Earth Surf. Process. Landf.* 27:773–787. doi:10.1002/esp.352.
- Schrott, L., and O. Sass. 2008. Application of field geophysics in geomorphology: Advances and limitations exemplified by case studies. *Geomorphology* 93:55–73. doi:10.1016/j.geomorph.2006.12.024.
- Sheehan, J.R., W.E. Doll, and W.A. Mandell. 2005. An evaluation of methods and available software for seismic refraction tomography analysis. *J. Environ. Eng. Geophys.* 10:21–34. doi:10.2113/JEEG10.1.21.
- Telford, W.M., L.P. Geldart, and R.E. Sheriff. 1990. *Applied geophysics*. 2nd ed. Cambridge Univ. Press, Cambridge, UK.
- Travelletti, J., J. Demand, M. Jaboyedoff, and F. Marillier. 2010. Mass movement characterization using a reflexion and refraction seismic survey with the sloping local base level concept. *Geomorphology* 116:1–10. doi:10.1016/j.geomorph.2009.10.006.
- Tye, A.M., H. Kessler, K. Ambrose, J.D.O. Williams, D. Tragheim, A. Scheib, M. Raines, and O. Kuras. 2011. Using integrated near-surface geophysical surveys to aid mapping and interpretation of geology in an alluvial landscape within a 3D soil-geology framework. *Near Surf. Geophys.* 9:15–31. doi:10.3997/1873-0604.2010038.
- Völkel, J., J. Huber, and M. Leopold. 2011. Significance of slope sediments layering on physical characteristics and interflow within the Critical Zone—Examples from the Colorado Front Range, USA. *Appl. Geochem.* 26:(Suppl. 1):S143–S145, doi:10.1016/j.apgeochem.2011.03.052
- Wobus, C.W., G.E. Tucker, and R.S. Anderson. 2010. Does climate change create distinctive patterns of landscape incision? *J. Geophys. Res.* 115(F4):F04008. doi:10.1029/2009JF001562.